THE JOURNAL OF PHYSICAL CHEMISTRY B

Article

pubs.acs.org/JPCB

Atomic Mechanism of Liquid−Glass Transition for Ca_7Mg_3 Alloy

Zhao-Yang Hou,[†,*] Li-Xia Liu,[‡] Ze-An Tian,[§] Rang-Su Liu,[∥] Yu Shu,[†] and Jin-Guo Wang[†]

[†]Department of Applied Physics, Chang'an University, Xi'an, 710064, China

[‡]Department of Mathematics, Xidian University, Xi'an 710071, China

[§]School of Materials Science and Engineering, University of New South Wales, Sydney, NSW 2052, Australia

[∥]School of Physics and Microelectronics Science, Hunan University, Changsha, 410082, China

ABSTRACT: The atomic mechanism of liquid−glass transition for Ca_7Mg_3 alloy during the rapid quenching processes is studied by the molecular dynamics simulations. The temperature dependences of structural, thermodynamic, and dynamic properties during the liquid−glass transition have been investigated. It is found that onset temperatures where these different properties begin to deviate from the equilibrium liquid are identical and near the melting temperature T_m. The liquid−glass transition temperatures in structure (T_g^{Str}) and dynamics (T_g^{Dyn}) are identical and higher than the calorimetric one (T_g^{Cal}), which are consistent with many experiments and computer simulations. The solid- and liquid-like atoms are defined by the Debye−Waller factor. It reveals that the solid-like atoms hold lower potential and higher degree of local order. On the basis of the evolution of solid-like atoms, the atomic mechanisms in structure, thermodynamics, and dynamics transition are systematically elucidated, which are consistent with the potential energy landscape.

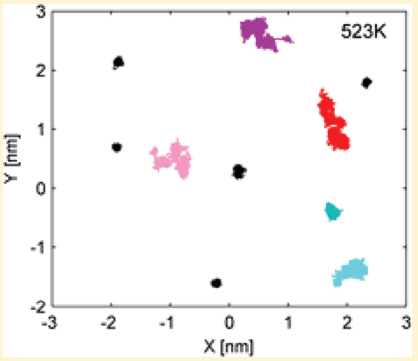

I. INTRODUCTION

The mechanism of liquid−glass transition has been extensively studied since the first metallic glass $Au_{75}Si_{25}$[1] was obtained by rapidly quenching the liquid melt. Many theoretical models such as the free volume theory,[2] configuration entropy theory,[3] and potential energy landscape[4] have been developed, and various degrees of successes especially in phenomenology have been made. However, the atomic mechanism of glass transition is still far from being fully understood.[5]

The liquid−glass transition is a complex process accompanied with structural, thermodynamic, and dynamic transitions. First, the structure quantities, as experimentally probed through the static structure factor or equivalently the pair distribution function (PDF), are believed to be gently dependent on the temperature. Recent reports[6−9] suggested that the short-range ordering (SRO) structures, especially the icosahedra, remarkably enhance during the liquid−glass transition, and play a critical role in the formation of glass structure. Second, the second-order thermodynamic quantities such as the coefficients of thermal expansion and specific heat change rapidly but continuously during the liquid−glass transition. Third, the dynamic quantities such as the transport coefficients of self-diffusion constant, viscosity, and relaxation time usually have much more pronounced temperature dependence, and often deviate from the well-known Arrhenius behavior below the melting temperature T_m. Phenomenologically, the temperature dependence of the dynamics close to the glass transition can be described quite well by the empirical Vogel−Fulcher−Tammann (VFT) law.[10−12] On the basis of the nonlinear coupling of density fluctuation, the mode-coupling theory (MCT)[13] predicts a dynamical singularity temperature T_c where the transition from ergodic to non-ergodic occurs. According to the critical changes in properties, different glass transition temperatures of T_g^{Str}, T_g^{Cal}, and T_g^{Dyn}, respectively, in structure, thermodynamics, and dynamics can be determined and their relationships have been investigated.[14−19] Lai and Chen[14] found that the T_g^{Dyn} is close to the T_g^{Str} determined by the PDF. Dzugutov et al.[15] found that the increase of icosahedra is arrested at around T_g^{Dyn}. Furthermore, many experiments and computer simulations[16−19] revealed that the T_g^{Dyn} is below the T_m and satisfies the relationship of $T_g^{Dyn} \approx 1.2T_g^{Cal}$. Although the relationships among the characteristic temperatures determined by different criteria have been investigated intensively, the knowledge about the underlying microscopic mechanisms of these relationships is still rather limited, which is important to deeply understand the nature of the liquid−glass transition.

Many experiments[20−23] have shown that the temperature dependence of the mean-square displacements displays a sharp change around the liquid−glass point in some polymer, biophysical, and oxide glass systems. This suggests that the liquid−glass transition is related to the atomic oscillation. On the basis of the Lindemann melting criterion for crystalline solids[24] that the melting occurs when the oscillation amplitude of atoms equals a universal fraction of the interatomic distance, Novikov et al.[25] defined the liquid- and solid-like atoms during the liquid−glass transition. Recently, Hoang[26,27] has further analyzed the spatial arrangements of solid- and liquid-like atoms

Received: February 16, 2012
Revised: June 10, 2012
Published: June 12, 2012

during the liquid−glass transition of the Lennard-Jones−Gauss (LJG) model system which promotes the formations of quasicrystal and complex crystal with its double wells.[28] However, the relationships between the atomic oscillation and the structural, thermodynamic, and dynamic transitions in metallic glasses need more investigations.

In a recent paper, we have deeply investigated the structural property of Ca_7Mg_3 metallic glass,[9] which is one of the few laboratory glass alloys composed of only two simple metallic elements.[29] Here we further study the evolutions of its structural, thermodynamic, and dynamic properties during the liquid−glass transition. The relationships among the transition temperatures determined by the different properties are also presented. Moreover, the atomic mechanism of the liquid−glass transition is revealed on the basis of the spatiotemporal properties of atomic oscillation. The organization of this paper is as follows: In section II, we describe the simulation methods. The results of our simulations are presented and discussed in section III. Finally, the summary is given in section IV.

II. SIMULATION METHODS

A. Interatomic Potentials. The Ca−Mg alloy is simulated with the effective pair potential derived from the generalized nonlocal model pseudopotential (GNMP) which is based upon the first-principle interaction force in the second-order perturbation theory.[30,31] The potential function is

$$V_{ij}(r) = \frac{Z_{\mathrm{eff},i}Z_{\mathrm{eff},j}}{r}\left\{1 - \left(\frac{1}{\pi}\right)\int_o^\infty \mathrm{d}q[F_{i,j}(q) + F_{j,i}(q)]\frac{\sin(rq)}{q}\right\} \quad (1)$$

where Z_{eff} and $F(q)$ are, respectively, the effective ionic valence and the normalized energy wavenumber characteristic, with details in refs 30 and 31. The potential is cut off at 20 au (atomic unit). For simple metals and their alloys, the accuracy and reliability of this potential have been extensively demonstrated by its computations of structural, dynamic, and thermodynamic properties.[30−33]

B. MD Simulation Methods. The rapid quenching process of Ca_7Mg_3 alloy is simulated by using the constant-pressure MD techniques.[33] The MD simulations are performed for a system containing 10 000 atoms (Ca:Mg = 7:3) in a cubic box with the periodic boundary condition. The motion equations are integrated through the leapfrog algorithm with a time step of 2.5 fs. The calculations start at 1123 K (the melting point T_m of Ca_7Mg_3 alloy is about 720 K). First of all, let the system run 50 000 time steps at 1123 K to obtain an equilibrium liquid determined by the energy change of system. Then, the damped force method[34−36] (also called the Gaussian thermostat) is adopted to decrease the system temperature to 273 K at a cooling rate of 1×10^{12} K/s. Every 50 K, the systems are isothermally relaxed 500 ps, respectively. During the quenching and relaxation processes, the temperature or the time dependences of velocities and positions for each atom are recorded to calculate the structural, dynamic, and thermodynamic quantities.

III. RESULTS AND DISCUSSION

A. Structural Liquid−Glass Transition. The PDF is widely used to detect the microstructural characteristics of liquids and glass solids. Figure 1 shows the total PDFs for the Ca_7Mg_3 alloy in the temperature range from 1123 to 273 K at an interval of 50 K. For the high-temperature liquid, the PDF curves display the typical liquid characteristics. With the decrease of temperature, the increase in height and the decrease in width of the first peak indicate the enhancement of SRO during the rapid quenching process. The second peak gradually splits into two subpeaks and the first subpeak grows higher than the second one, which indicates the formation of Ca_7Mg_3 metallic glass. Through the Fourier transformation of RDF, the structure factor $S(Q)$ for the simulated Ca_7Mg_3 metallic glass at 323 K is obtained and depicted in Figure 2,

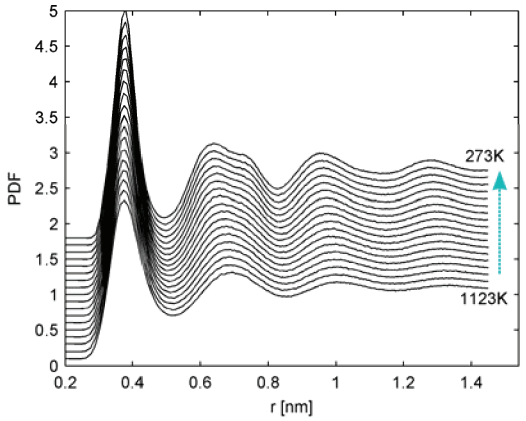

Figure 1. Total PDFs for the Ca_7Mg_3 alloy in the temperature range from 1123 to 273 K at an interval of 50 K.

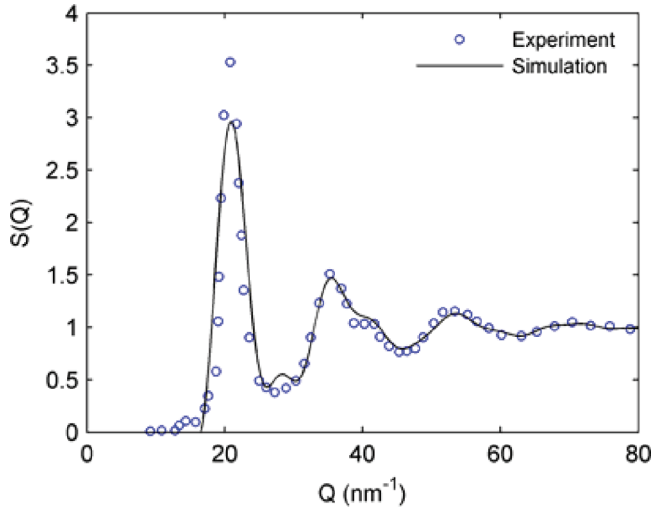

Figure 2. Comparison of $S(Q)$ for Ca_7Mg_3 metallic glass at 323 K between the simulation and experiment.

together with the experimental data.[37] It can be found that the simulation results agree well with the experiment except for the slight difference at the first peak. Considering the fact that the much faster cooling rate in our simulations reduces the degree of SRO in metallic glasses and lowers the height of the first peak of $S(Q)$ evidently,[38] our calculations are pretty accurate in simulating the rapid quenching process of Ca_7Mg_3 alloy.

The glass transition point is difficult to be determined directly by the PDFs in Figure 1, since the PDF only gently depends on temperature. Wendt and Abraham[39] proposed an empirical but widely used criterion to identify the glass transition point by means of the height ratio between the

dx.doi.org/10.1021/jp301576f | J. Phys. Chem. B 2012, 116, 7746−7753

first minimum and the first maximum of the total PDF, i.e., $R = g_{min}/g_{max}$. R varies linearly with the temperature in both the liquid and glass regions with different slopes, respectively, and the glass transition point is defined by the intersection of the extrapolations of the two linear plots. From the temperature dependence of the Wendt−Abraham ratio R of Ca_7Mg_3 alloy, as shown in Figure 3, the glass transition temperature is estimated to be 540 K.

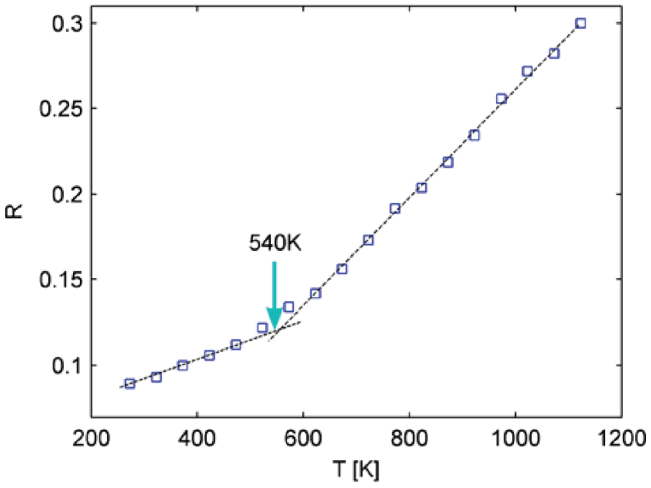

Figure 3. Temperature dependence of the Wendt−Abraham ratio R during the liquid−glass transition of Ca_7Mg_3 alloy.

Further to the one-dimensional (1D) description of microstructures presented by the PDF, the 3D information of the topological SRO in the Ca_7Mg_3 metallic glass has recently been identified by several structural analysis methods.[9] Our results reveal that the icosahedron, especially the Mg-centered icosahedron, is the favorable SRO structure. Figure 4 further

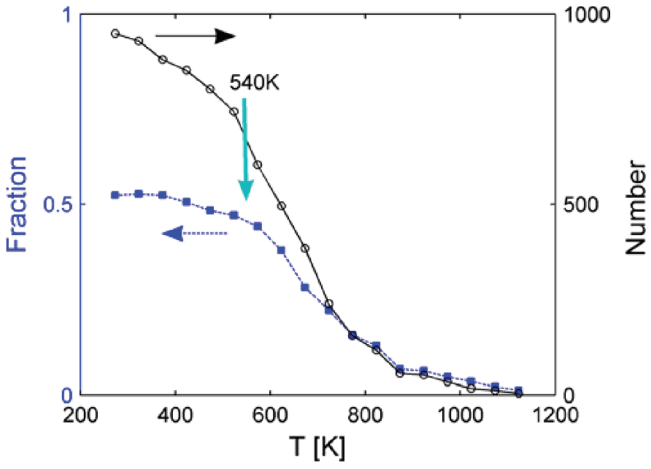

Figure 4. Temperature dependences of the number of icosahedra (solid line) and the percent of atoms involved in all icosahedra (dashed line) during the liquid−glass transition of Ca_7Mg_3 alloy.

shows the temperature dependences of the number of icosahedra and the percent of atoms involved in all icosahedra during the liquid−glass transition process. It can be found that they both strongly depend on the temperature. The number of icosahedra is very few in the high temperature liquid as $T > 873$ K and then grows rapidly until cooling to about 540 K. Meanwhile, the proportion of atoms involved in all icosahedra reaches 58.8% and changes slightly thereafter. Therefore, the icosahedron plays a critical role in the formation of Ca_7Mg_3 metallic glass, and the glass structure is formed at around 540 K. The glass transition point obtained by the change of SRO units is the same as that obtained by the Wendt−Abraham ratio, i.e., the glass transition temperature in structure $T_g^{Str} \approx$ 540 K.

B. Thermodynamic Liquid−Glass Transition. Figure 5 displays the temperature dependence of potential energy per

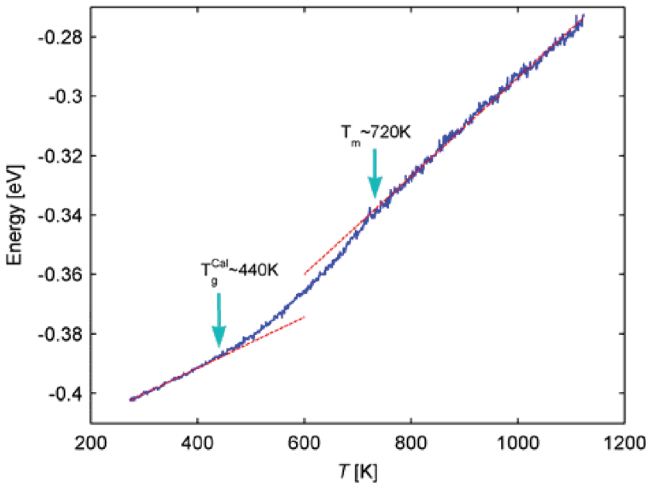

Figure 5. Temperature dependence of potential energy per atom during the liquid−glass transition of Ca_7Mg_3 alloy. The straight dashed lines serve as a guide to the eyes.

atom of Ca_7Mg_3 alloy. The potential energy curve begins to deviate from linearity around $T_m \approx 720$ K, and a new linear relationship rebuilds up at about 440 K. This indicates that the system begins to fall out of the equilibrium liquid near T_m, and the glass solid forms at around 440 K, i.e., the calorimetric glass transition temperature $T_g^{Cal} \approx 440$ K, which is lower than $T_g^{Str} \approx 540$ K.

C. Dynamic Liquid−Glass Transition. The mean-square displacement (MSD)[40] is usually used to study the dynamic motion of atoms, which is defined as

$$\langle r^2(t)\rangle = \frac{1}{N}\sum_{i=1}^{N}\langle |r_i(t) - r_i(0)|^2\rangle \quad (2)$$

where N is the number of atoms in a system; $r_i(0)$ and $r_i(t)$ are the position vectors of the ith atom at the initial moment and the time t, respectively. Since the time dependences of MSD for Ca and Mg atoms are very similar, for clarity, we only display the MSD for Mg at different temperatures in Figure 6. At the high temperatures, the MSD shows the characteristics of simple liquid, i.e., a quadratic dependence on short time due to the vibration of atoms, and a linear change in the following stage for the diffusive motion of atoms.[41] At the lower temperatures, a plateau appears in the intermediate time window and becomes more and more pronounced with decreasing temperature. The occurrence of this plateau results from the so-called "cage effect" of tagged atoms. The tagged atom needs some time to escape from the cage formed by its neighboring atoms, and the cage becomes more and more rigid with decreasing temperature. Thus, the time needed to escape from the cage increases correspondingly. In the MCT,[13] the time window

dx.doi.org/10.1021/jp301576f | J. Phys. Chem. B 2012, 116, 7746−7753

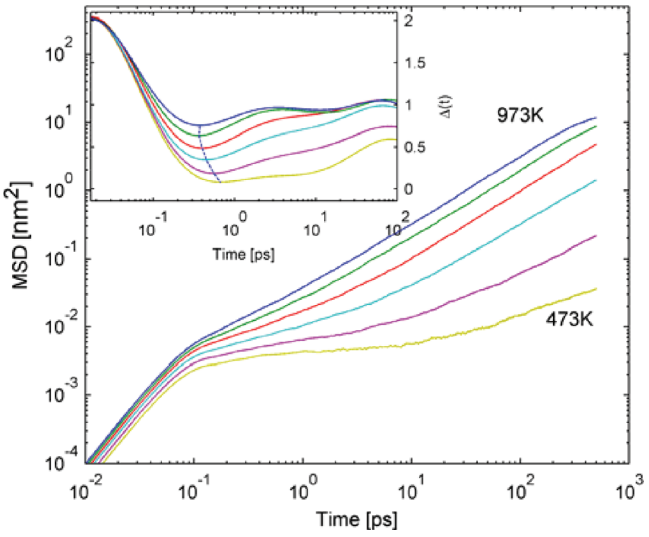

Figure 6. Time dependence of MSD for Mg in Ca_7Mg_3 alloy on a double logarithmic scale at different temperatures. The temperature varies from 973 K (top) to 473 K (bottom) at an interval of 100 K. Inset: changes of corresponding MSD slope $\Delta(t) = \partial \log\langle r^2(t)\rangle/\partial \log t$ with the relaxation time; the dashed line shows the position of the minimums of $\Delta(t)$.

correlated with the cage effect is usually called the β-relaxation regime and the following time window is the α-relaxation regime.

The MSD can be used to calculate the self-diffusion coefficient D according to the Einstein relation

$$D = \lim_{t\to\infty} \frac{1}{6t}\langle r^2(t)\rangle \tag{3}$$

The temperature dependences of D for Ca and Mg atoms are shown in Figure 7, together with the fits by the Arrhenius law (eq 4), VFT law[10−12] (eq 5), and MCT power law[13] (eq 6), respectively, in different temperature regions.

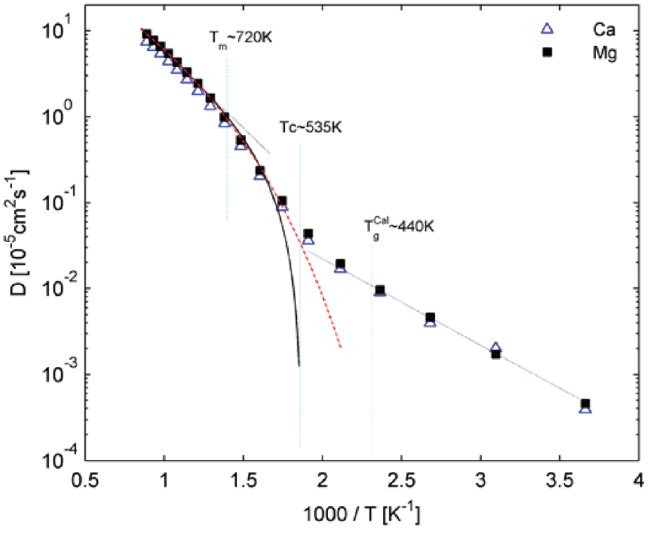

Figure 7. Temperature dependences of self-diffusion coefficient D in an Arrhenius plot during the liquid−glass transition of Ca_7Mg_3 alloy. The dashed (blue), dash dotted (red), and solid lines (black) are the Arrhenius, VFT, and MCT fits of D, respectively.

$$D(T) = D_0^{\mathrm{Arrh}} \exp[-Q^{\mathrm{Arrh}}/RT] \tag{4}$$

$$D(T) = D_0^{\mathrm{VFT}} \exp[-Q^{\mathrm{VFT}}/(T - T_{\mathrm{VFT}})] \tag{5}$$

$$D(T) \sim |T - T_c|^{\gamma} \tag{6}$$

The fitting parameters in eqs 4−6 are listed in Table 1. The $D(T)$ curves for Ca and Mg are very similar, so only the fitting curves for Mg are shown in Figure 7 for clarity. The temperature dependence of D can be divided into three temperature regimes.

Table 1. Fitting Parameters for Self-Diffusion Coefficients by Using the Arrhenius, VFT, and MCT Laws, Respectively

fitting law	parameter	Ca	Mg
Arrhenius (T > 673 K)	D_0^{Arrh} (cm²/s)	3.00×10^{-3}	2.02×10^{-5}
	Q^{Arrh} (J/mol)	34330	10970
MCT (T > 473 K)	T_c (K)	534	535
	γ	1.86	1.86
VFT (T > 423 K)	D_0^{VFT} (cm²/s)	8.11×10^{-4}	9.78×10^{-4}
	Q^{VFT} (J/mol)	16632	16504
	T^{VFT} (K)	285	288
Arrhenius (T < 423 K)	D_0^{Arrh} (cm²/s)	3.68×10^{-3}	2.27×10^{-5}
	Q^{Arrh} (J/mol)	34411	19226

The first stage is for liquid with $T > T_m$, and it follows the Arrhenius law (eq 4). The activation energy of Mg is smaller than Ca (see Q^{Arrh} in Table 1), which indicates that the smaller Mg atom diffuses faster than the bigger Ca.

In the second stage ($T_m > T > T_c$), upon cooling from T_m, D drops faster, deviating from the Arrhenius law while well fitted by the MCT power law (eq 6) until 573 K, with $\gamma = 1.86$ and $T_c \approx 535$ K for both Ca and Mg. This is reasonably well fulfilled in the prediction of MCT that the exponent γ and critical temperature T_c should be independent of the atomic species.[41] In addition, the self-diffusion coefficient D is well fitted by the VFT law (eq 5) before the temperature decreases to 523 K which is close to the MCT critical temperature $T_c \approx 535$ K. This analysis shows that the MCT only gives a fair representation of the diffusivity down to 573 K $\approx 1.07T_c$, while the VFT law can describe the diffusivity above T_c. Our findings coincide with the result of the bulk glass-forming Cu−Ti−Zr alloy[42] but are slightly different from that for the Lennard-Jones model system[43] where the MCT power law turned out to be superior to the VFT relationship when restricting to the temperature $T \geq 1.07T_c$.

In the third stage for glass solid with $T < T_c$, the self-diffusion coefficient D follows the Arrhenius law (eq 4) again with a different set of fitting parameters. The diffusion activation energies (Q^{Arrh}) of Mg and Ca atoms are both larger than those in the high-temperature liquid above T_m. This indicates that the diffusion in the glass solid is more difficult than that in the liquid.

From the above dynamic analysis, the crossover temperature between liquid-type and solid-type dynamics is around T_c, i.e., the dynamic glass transition temperature $T_g^{\mathrm{Dyn}} = T_c \approx 535$ K. It is very close to $T_g^{\mathrm{Str}} \approx 540$ K and equal to $1.22T_g^{\mathrm{Cal}}$. The relationships among T_g^{Str}, T_g^{Cal}, and T_g^{Dyn} are consistent with many other experiments and simulations.[14−19]

The non-Gaussian parameter (NGP)[44] is frequently used to quantify the dynamic heterogeneity of supercooled liquid, and is defined as

dx.doi.org/10.1021/jp301576f | J. Phys. Chem. B 2012, 116, 7746−7753

$$\alpha_2(t) = \frac{3\langle r^4(t)\rangle}{5\langle r^2(t)\rangle^2} - 1 \quad (7)$$

where $\langle r^4(t)\rangle$ is the mean quartic displacement. The time dependences of NGP for Mg in the Ca_7Mg_3 alloy at different temperatures are shown in Figure 8. For short time (t < 0.1 ps),

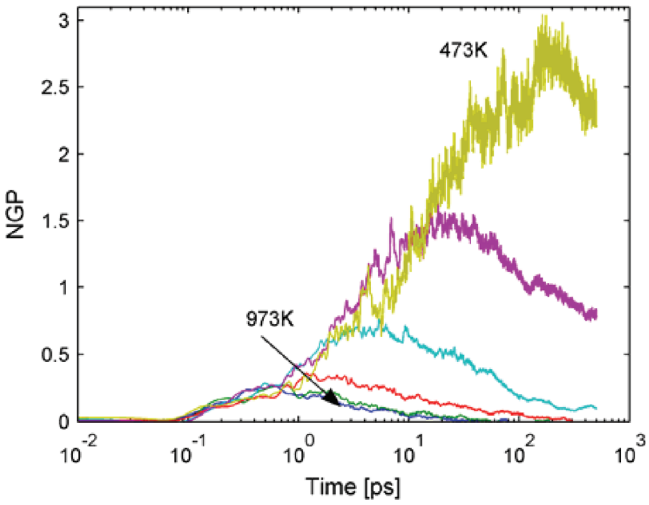

Figure 8. Time dependence of NGP for Mg in the Ca_7Mg_3 alloy at different temperatures. The temperature varies from 973 K (bottom) to 473 K (top) at an interval of 100 K.

all NGPs at different temperatures are zero, which indicates that the vibration of atoms follows the Gaussian distribution. During the β-relaxation regime, all the NGP curves rise monotonically to a maximum due to the cooperative motion of cage atoms. The positions of maximum NGP shift toward longer time with the decrease of temperature, suggesting the increase of dynamic heterogeneity. During the α-relaxation regime, the NGP curves drop down with the cage-breaking rearrangement, and their descending rates vary with the temperature. For the supercooled liquid above T_m, the NGP curves finally drop to zero due to the diffusion motion of atoms. Below T_c, the glassy solid is incapable of relaxing because the relaxation times are much longer than the scale of simulation time; thus, the motion of atoms is nonergodic and the NGP curves at 473 K cannot drop to zero.

D. Solid- and Liquid-Like Atoms. Upon approaching the glass transition, the motion of atoms is localized within the cages formed by their neighbors, showing up as a plateau in the MSD curves in Figure 6. The rattling motion inside the cage occurs in a short time with the amplitude $\langle u^2\rangle$, the so-called Debye–Waller (DW) factor. The DW factor is usually experimentally obtained by using the intermediate scattering function[45] and can be extracted from the MSD in the time window where neither the inertial nor relaxation effects are presented.[46,47] To identify the time window for the DW factor, we plot the changes of MSD slope in the log–log plot, i.e., $\Delta(t) = \partial \log\langle r^2(t)\rangle/\partial \log t$, in the inset of Figure 6. At the short time limit, $\Delta(t)$ is 2 for all different temperatures, corresponding to the ballistic motion of atoms. At the long time limit, $\Delta(t) = 1$ for the supercooled liquid above T_m due to the diffusive motion of atoms. $\Delta(t)$ exhibits a clear minimum at t^* where an inflection point separates the two regimes. Also, similar to that in the polymer and colloid systems,[46,47] t^* changes slightly with temperature. Therefore, the MSD value at t^* (about 0.48 ps) reflects the mean localization length, and the DW factor $\langle u^2\rangle$ is defined as

$$\langle u^2\rangle = \langle r^2(t = t^*)\rangle \quad (8)$$

Figure 9 shows the temperature dependences of the DW factors $\langle u^2\rangle$ for Ca and Mg atoms during the liquid–glass

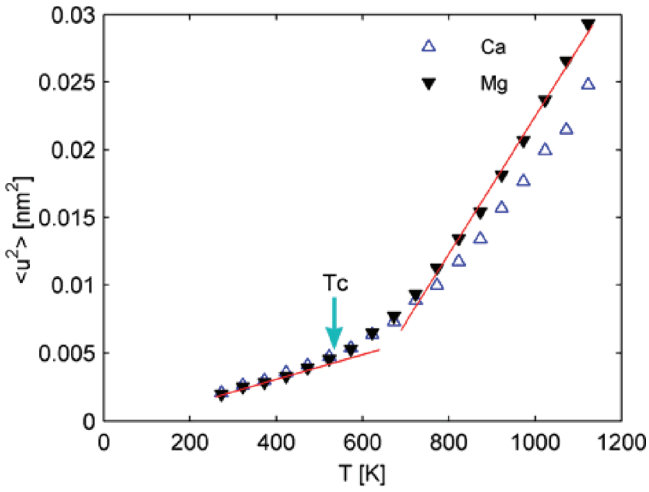

Figure 9. Temperature dependences of the DW factors $\langle u^2\rangle$ for Ca and Mg atoms during the liquid–glass transition of Ca_7Mg_3 alloy. The straight lines for Mg serve as a guide to the eyes.

transition of Ca_7Mg_3 alloy. The DW factors decrease linearly both in the liquid ($T > T_m$) and glass solid ($T < T_c$), as expected from the equipartition theorem. This suggests that the glass solid has formed when the DW factor reaches the critical value $\langle u_c^2\rangle$ at T_c. Just as the Lindemann melting criterion for crystalline solids,[24] the corresponding Lindemann ratios δ_L for Ca and Mg atoms are equal to 0.20 and 0.24, respectively. Both of them are larger than those of fcc crystal δ_L = 0.13 and bcc crystal δ_L = 0.18. Up to now, the experimental data of Lindemann ratios for the glass-forming system are still deficient, and our simulation results are close to that (δ_L = 0.21) obtained by Hoang[26,27] for the LJG system.

Due to the structural fluctuation in the supercooled liquid, the rattling amplitude of each atom may be different. Those whose rattling amplitudes are smaller than $\langle u_c^2\rangle$ are defined as solid-like atoms; otherwise, they are liquid-like. We regard that two solid-like atoms are in one cluster if their distance is within the range of first minimum in the RDF. Figure 10 shows the evolution of the solid-like atoms during the liquid–glass transition. When $T > T_m$, the solid-like atoms are very scarce, and most of them are isolated from each other (see Figure 10a and b). Upon cooling from T_m, the solid-like atoms begin to increase remarkably, and the largest solid cluster including most solid-like atoms spreads into the whole simulation box (see Figure 10a and c). At 523 K (closing to T_g^{Dyn}), the largest solid cluster already involves 74.2% atoms of the system (Figure 10d and e). From 423 K (closing to T_g^{Cal}), the solid-like atoms increase slowly. The largest solid cluster involves 92.6% atoms, which indicates that the system becomes a rigid glassy solid.

E. Atomic Mechanism of Liquid–Glass Transition. According to the above analyses, the onset temperature T_m where the system begins to deviate from the equilibrium liquid is identical when it is determined from different aspects. The glass transition temperatures in structure and dynamics are also

dx.doi.org/10.1021/jp301576f | J. Phys. Chem. B 2012, 116, 7746–7753

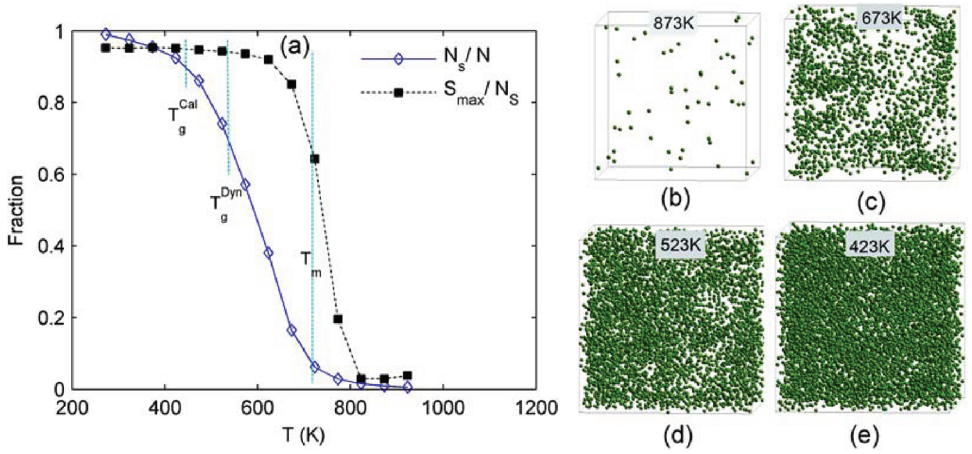

Figure 10. Evolutions of solid-like atoms during the liquid−glass transition of Ca_7Mg_3 alloy. (a) The proportion of solid-like atoms in the system (N_s/N) and the ratio in the number of solid-like atoms in the largest solid cluster to all (N_{max}/N_s). (b−e) Schematics of the distribution of solid-like atoms in the simulation box at different temperatures.

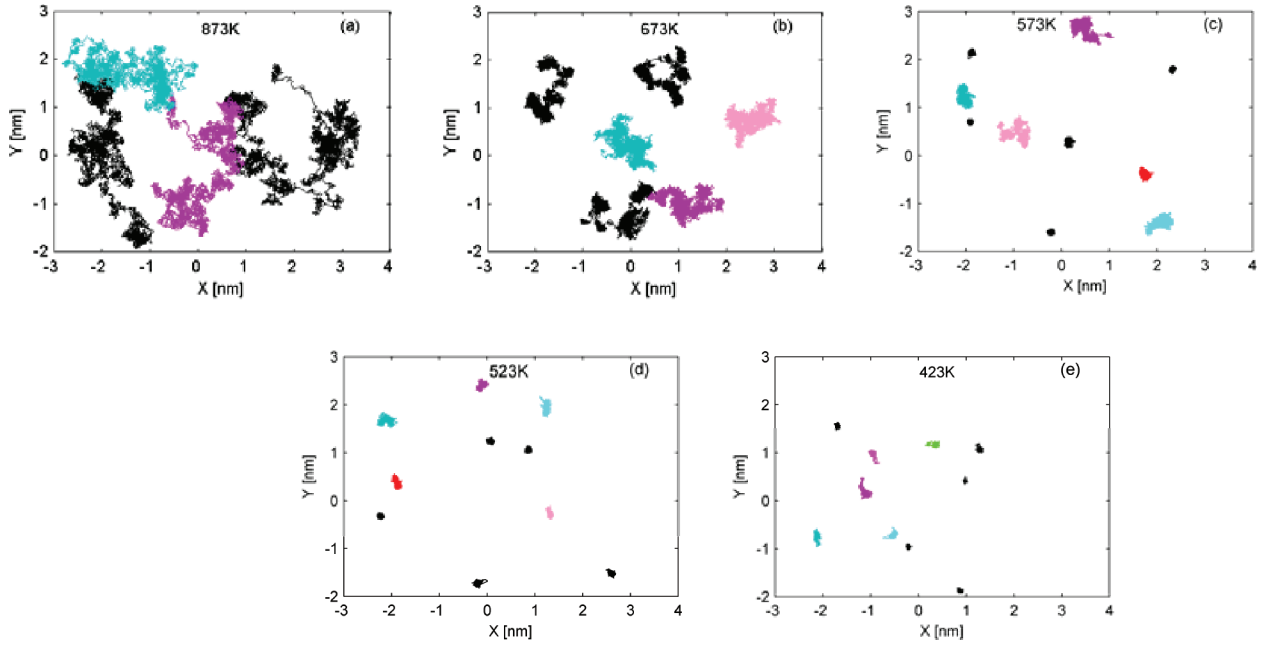

Figure 11. Trajectories of some solid- and liquid-like atoms over 500 ps projected onto the *XY* plane at different temperatures. In each panel, the black color is for solid-like atoms, and other colors are for liquid-like atoms.

identical, $T_g^{Str} \approx T_g^{Dyn} \approx 540$ K, which is higher than the calorimetric one, $T_g^{Cal} \approx 440$ K. To further elucidate the atomic mechanisms in structure, thermodynamics, and dynamics during the liquid−glass transition, the properties of solid- and liquid-like atoms are investigated as follows.

Figure 11 shows the trajectories of the some solid- and liquid-like atoms over 500 ps projected onto the *XY* plane at different temperatures. As $T > T_m$, both the solid- and liquid-like atoms are active and show liquid flowing (see Figure 11a). Upon cooling from T_m, the situation becomes quite different. The solid-like atoms are immobile and vibrate locally around their original positions due to the cage effect, while the liquid-like atoms are relatively mobile and hop multiple times away from the cages (see Figure 11b and c). When $T < T_g^{Dyn}$, both the solid- and liquid-like atoms vibrate locally around their original positions (Figure 11d and e) and their rattling amplitudes (in the *XY* plane) are very small, about one atomic distance. Thus, the self-diffusion coefficients in Figure 7 show the Arrhenius behavior as $T > T_m$, and then exhibit the non-Arrhenius behavior due to the cage effect. The dynamic singularity point T_g^{Dyn} is reached when all atoms are difficult to escape from the cages.

From the potential energy distributions of the solid- and liquid-like Mg atoms at 523 K, as shown in Figure 12, it can be found that the three distributions differ by a small relative shift of the most probable value, and the most probable energy of the solid-like atoms is lower than that of the liquid-like ones. We also find that the shift magnitude of the most probable energy increases with the decrease of temperature (not shown). Therefore, when the solid-like atoms appear remarkably near T_m (see Figure 10), the thermodynamic property (potential energy per atom in Figure 5) of the system falls out of the equilibrium liquid gradually, and a new thermodynamic equilibrium is established when the solid-like atoms become dominated at around T_g^{Cal}.

dx.doi.org/10.1021/jp301576f | J. Phys. Chem. B 2012, 116, 7746−7753

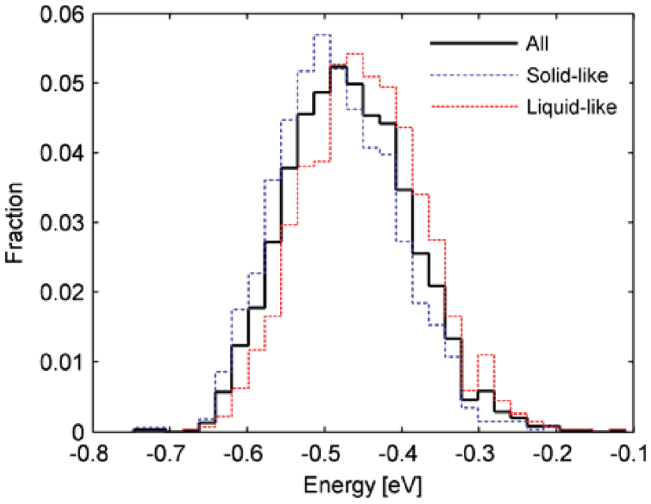

Figure 12. Potential energy distributions of all Mg atoms, the solid- and liquid-like Mg atoms at 523 K. Each distribution has been normalized; i.e., the areas under each curve are 1.

From the distributions of the rattling amplitudes $\langle u^2\rangle^{1/2}$ for all Mg atoms and the Mg atoms centered icosahedra at 523 K, as shown in Figure 13, it can be found that most icosahedra are

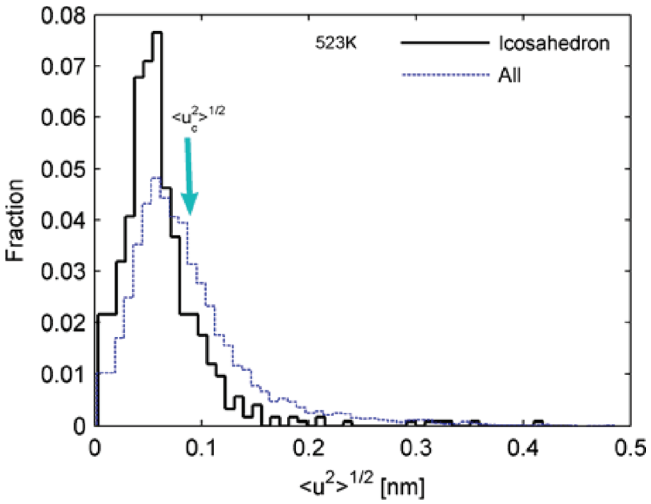

Figure 13. Distributions of rattling amplitudes $\langle u^2\rangle^{1/2}$ of all Mg atoms and the Mg atoms centered icosahedra at 523 K. Each distribution has been normalized, i.e. the areas under each curve are 1.

solid-like atoms with lower mobility. Together with the lower local energy of icosahedra (as shown in ref 9), it can be concluded that the SRO structures with icosahedral order are favorable during the liquid−glass transition. As $T > T_m$, most atoms (even solid-like atoms) have larger rattling amplitudes (see Figure 14), and this suggests larger structural fluctuation in the high temperature liquid. Thus, the canonical icosahedra are difficult to form as $T > T_m$ (see Figure 4), while lots of SRO structures with defective icosahedral order are formed (see Figure 6 of ref 9). Upon cooling from 523 K (being close to T_g^{Dyn}), even the liquid-like atoms have small rattling amplitudes; thus, most solid-like atoms together with many liquid-like atoms are icosahedral atoms (see Figure 13). Since most atoms are involved in icosahedra when $T < T_g^{Dyn}$, the increase of icosahedra becomes very slow from then on.

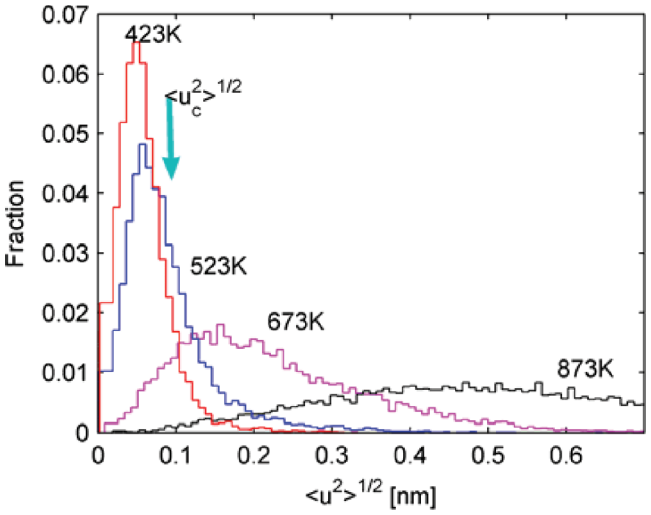

Figure 14. Distributions of rattling amplitudes $\langle u^2\rangle^{1/2}$ of Mg atoms at different temperatures. For clarity, the rattling amplitude is truncated at 0.7 nm. Each distribution has been normalized; i.e., the areas under each curve are 1.

With lower mobility and potential energy, the solid-like atoms can be regarded as being in the metabasins of the potential energy landscape.[4,18] When $T > T_m$, the solid-like atoms are few (see Figure 10), and the differences in potential energy between the solid- and liquid-like atoms are also little. These suggest that the metabasins are very shallow and most atoms have sufficient kinetic energy to sample the entire energy landscape. Thus, both the solid- and liquid-like atoms can move stochastically in the entire simulation space (see Figure 11a), and the temperature dependence of the self-diffusion coefficients D exhibits the Arrhenius behavior with lower activation energy (see Figure 7). Upon cooling from T_m, the number of solid-like atoms increases remarkably and most of them connect with each other (see Figure 10). This means that more and deeper metabasins are formed in the system, which increases the activation energy of atoms. Therefore, the solid-like atoms are difficult to escape from the metabasins and locally vibrate around their original positions, while the liquid-like atoms need a longer waiting time to jump away from their original positions (see Figure 11c). The depth of the metabasin is further strengthened as the solid-like atoms are dominant in the glass solid with $T < T_g^{Dyn}$ (see Figure 10). Thus, most atoms including many liquid-like ones are localized into the deeper metabasins, and vibrate around their original positions (see Figure 11e).

Comparing to the LJG system,[26,27] it can be found that for the LJG system the temperature dependence of the self-diffusion coefficient changes sharply between the liquid and glass Arrhenius behaviors; that is, the temperature window for the MCT power law is difficult to be observed (see Figure 1 in ref 26). This indicates that the LJG system is a strong glass former, while the Ca_7Mg_3 alloy is a fragile one.[41] Furthermore, according to the temperature dependences of the potential energy (see Figure 2 in ref 26) and the fraction of bond-pair (see Figure 2 in ref 27) in the LJG system, both the structural and thermodynamic properties begin to deviate from the equilibrium liquid near the MCT critical temperature T_c. The glass transition temperatures in structure and thermodynamics are identical, labeled as T_g by Hoang,[26,27] and they are lower than the dynamic one. The relationships among these

dx.doi.org/10.1021/jp301576f | J. Phys. Chem. B 2012, 116, 7746−7753

characteristic temperatures for the LJG system are obviously different from those for the present Ca_7Mg_3 metallic alloy and many others.[14−19] Moreover, Hoang[26,27] suggested that the solid-like atoms appear only below T_c at which the dynamics property of the system already presents solid type. Obviously, our result is different from their arguments, and this may be caused by the different strategies of choosing the characteristic time t^* in eq 8. The t^* chosen by Hoang corresponds to the end of the plateau regime on the MSD curve, where the relaxation effects have been fully presented. The longer characteristic time t^* used in our calculation can produce larger rattling amplitudes of atoms, and more atoms are classified as the liquid-like atoms.

IV. CONCLUSION

To understand the atomic mechanism of the liquid−glass transition, a molecular dynamics simulation for Ca_7Mg_3 alloy has been performed on the rapid quenching processes, based on the effective pair potential derived from the generalized nonlocal model pseudopotential theory. The evolutions of the structure, thermodynamics, and dynamics properties are investigated. It is found that the onset temperatures where these different properties begin to deviate from the equilibrium liquid are identical and near T_m. The liquid−glass transition temperatures determined from the structural and dynamic properties are identical, $T_g^{Str} \approx T_g^{Dyn} \approx 540$ K. They are higher than the calorimetric one, $T_g^{Cal} \approx 440$ K, and equal to $1.22T_g^{Cal}$. The relationships among T_g^{Str}, T_g^{Cal}, and T_g^{Dyn} are consistent with many other experiments and simulations but different from that in the LJG model system. The investigations on the solid-like atoms defined by the Debye−Waller factor show that the solid-like atoms with lower mobility possess lower potential energy and favor icosahedral order. The atomic mechanisms of liquid−glass transition in structure, thermodynamics, and dynamics are further elucidated systematically according to the evolution of solid-like atoms with the decrease of the temperature. Also, it is consistent with the potential energy landscape of the liquid−glass transition.

AUTHOR INFORMATION

Corresponding Author

*E-mail: zhaoyanghou@163.com, houzhaoyang@gmail.com.

Notes

The authors declare no competing financial interest.

ACKNOWLEDGMENTS

The authors give grateful thanks for the support of National Natural Science Foundation of China (Grant Nos. 51101022 and 50831003) and the Special Fund for Basic Scientific Research of Central Colleges (Grant Nos. CHD2012JC096 and K50511700006).

REFERENCES

(1) Klement, W.; Willens, R. H.; Duwez, P. *Nature* **1960**, *187*, 869−870.
(2) Cohen, M. H.; Grest, G. S. *Phys. Rev. B* **1979**, *20*, 1077−1098.
(3) Adam, G.; Gibbs, J. H. *J. Chem. Phys.* **1965**, *43*, 139−146.
(4) Goldstein, M. *J. Chem. Phys.* **1969**, *51*, 3728−3739.
(5) Anderson, P. W. *Science* **1995**, *17*, 1609−1618.
(6) Tomida, T.; Egami, T. *Phys. Rev. B* **1995**, *52*, 3290−3308.
(7) Kelton, K. F.; Gangopadhyay, A. K.; Kim, T. H.; Lee, G. W. *J. Non-Cryst. Solids* **2006**, *352*, 5318−5324.
(8) Cheng, Y. Q.; Sheng, H. W.; Ma, E. *Phys. Rev. B* **2008**, *78*, 014207.
(9) Hou, Z. Y.; Liu, L. X.; Liu, R. S.; Tian, Z. A.; Wang, J. G. *J. Appl. Phys.* **2010**, *107*, 083511.
(10) Vogel, H. *Phys. Z.* **1921**, *22*, 645−646.
(11) Fulcher, G. S. *J. Am. Ceram. Soc.* **1925**, *8*, 339−355.
(12) Tammann, G.; Hesse, G. *Z. Anorg. Allg. Chem.* **1926**, *156*, 245−257.
(13) Gőtze, W.; Sjőgren, L. *Rep. Prog. Phys.* **1992**, *55*, 241−376.
(14) Lai, S. K.; Chen, H. C. *J. Phys: Condens. Matter* **1993**, *5*, 4325−4342.
(15) Dzugutov, M.; Simdyankin, S. I.; Zetterling, F. H. M. *Phys. Rev. Lett.* **2002**, *89*, 195701.
(16) Angell, C. A. *J. Phys. Chem. Solids* **1988**, *49*, 863−871.
(17) Mohanty, U.; Diezemann, G.; Fourkas, J. T. *J. Chem. Phys.* **2000**, *113*, 3719−3722.
(18) Debenedetti, P. G.; Stillinger, F. H. *Nature* **2001**, *410*, 259−267.
(19) Odagaki, T. *Phys. Rev. Lett.* **1995**, *75*, 3701−3704.
(20) Angell, C. A. *Science* **1995**, *267*, 1924−1935.
(21) Frick, B.; Richter, D. *Phys. Rev. B* **1993**, *47*, 14795−14804.
(22) Doster, W.; Cusak, S.; Petry, W. *Nature* **1989**, *337*, 754−756.
(23) Engberg, D.; Wischnewski, A.; Buchenau, U.; Borjesson, L.; Dianoux, A. J.; Sokolov, A. P.; Torell, L. M. *Phys. Rev. B* **1998**, *58*, 9087−9097.
(24) Lindemann, F. A. *Z. Phys.* **1910**, *11*, 609−612.
(25) Novikov, V. N.; Rőssler, E.; Malinovsky, V. K.; Surovtsev, N. V. *Europhys. Lett.* **1996**, *35*, 289−294.
(26) Hoang, V. V.; Odagaki, T. *Solid State Commum* **2010**, *150*, 1971−1975.
(27) Hoang, V. V.; Odagaki, T. *J. Phys. Chem. B* **2011**, *115*, 6946−6956.
(28) Engel, M.; Trebin, H. R. *Phys. Rev. Lett.* **2007**, *98*, 225505.
(29) Hafner, J. *Phys. Rev. B* **1980**, *21*, 406−426.
(30) Wang, S.; Lai, S. K. *J. Phys. F* **1980**, *10*, 2717−2737.
(31) Li, D. H.; Li, X. R.; Wang, S. *J. Phys. F* **1986**, *16*, 309−321.
(32) Wang, S.; Lai, S. K.; So, C. B. *J. Phys. F* **1980**, *10*, 445−459.
(33) Jin, Z. H.; Lu, K.; Gong, Y. D.; Hu, Z. Q. *J. Chem. Phys.* **1997**, *106*, 8830−8840.
(34) Hoover, W. G.; Ladd, A. J. C.; Moran, B. *Phys. Rev. Lett.* **1982**, *48*, 1818−1820.
(35) Evans, D. J. *J. Chem. Phys.* **1983**, *78*, 3297−3302.
(36) Brown, D.; Clarke, J. H. R. *Mol. Phys.* **1984**, *51*, 1243−1252.
(37) Nassif, E.; Lamparter, P.; Steev, S. *Z. Naturforsch., Sect. A* **1983**, *38*, 1206−1209.
(38) Vollmayr, K.; Kob, W.; Binder, K. *Phys. Rev. B* **1996**, *54*, 15808−15827.
(39) Wendt, H. R.; Abraham, F. F. *Phys. Rev. Lett.* **1978**, *41*, 1244−1246.
(40) Allen, M. P.; Tildesley, D. J. *Computer Simulation of Liquids*; Oxford University Press: New York, 1989.
(41) Kob, W. *J. Phys.: Condens. Matter* **1999**, *11*, R85−R115.
(42) Han, X. J.; Teichler, H. *Phys. Rev. E* **2007**, *75*, 061501.
(43) Kob, W.; Andersen, H. C. *Phys. Rev. Lett.* **1994**, *73*, 1376−1379.
(44) Rahman, A. *Phys. Rev.* **1964**, *136*, A405−A411.
(45) Ngai, K. L. *J. Non-Cryst. Solids* **2000**, *275*, 7−51.
(46) Ottochian, A.; De Michele, C.; Leporini, D. *J. Chem. Phys.* **2009**, *131*, 224517.
(47) De Michele, C.; Del Gado, E.; Leporini, D. *Soft Matter* **2011**, *7*, 4025−4031.